Ground, Ceiling and Wall Effect Evaluation of Small Quadcopters in Pressure-controlled Environments

Journal of Intelligent & Robotic Systems (2024) 110:125
https://doi.org/10.1007/s10846-024-02155-7

REGULAR PAPER

Ground, Ceiling and Wall Effect Evaluation of Small Quadcopters in Pressure-controlled Environments

Iris David Du Mutel de Pierrepont Franzetti[1,2] · Riccardo Parin[2] · Elisa Capello[3] · Matthew J. Rutherford[4] · Kimon P. Valavanis[5]

Received: 20 December 2023 / Accepted: 23 July 2024 / Published online: 24 August 2024

Abstract
Multicopters are used for a wide range of applications that often involve approaching buildings or navigating enclosed spaces. Opposed to the open spaces in obstacle-free environments commonly flown by fixed-wing unmanned aerial vehicles, multicopters frequently fly close to surfaces and must take into account the airflow variations caused by airflow rebound. Such disturbances must be identified in order to design algorithms capable of compensating them. The evaluation of ground, ceiling and wall effects using two different test stands is proposed in this work. Different propellers and sensors have been considered for testing. The first test setup used was placed inside terraXcube's large climatic chamber allowing a precise control of temperature and pressure of around 20°C and 1000 hPa, respectively. The second test setup is located at the University of Denver (DU) Unmanned Systems Research Institute (DU^{2}SRI) laboratory with a stable pressure of around 800 hPa. Two different fixed 6 degrees of freedom force-torque sensors have been used for the experiments, allowing to sample forces and moments in three orthogonal axes. The tests simulate a hovering situation of a quadcopter at different distances to either the ground, the ceiling or a wall. The influence of the propeller size, rotation speed, pressure and temperature have also been considered and used for later dimensionless coefficient comparison. A thorough analysis of the measurement uncertainty is also included based on experimental evaluations and manufacturer information. Experimental data collected in these tests can be used for the definition of a mathematical model in which the effect of the proximity to the different surfaces is evaluated.

Keywords Unmanned aerial vehicle · Wall effect · Ground effect · Ceiling effect · Quadrotor · Autonomous vehicles · Disturbance modelling

1 Introduction

The use of multicopters in indoor environments is becoming more common due to the automation of simple tasks such as surveillance [1] or warehouse activities [2, 3]. Particularly for indoor environments where GPS signal is frequently weak or absent, unmanned aerial vehicles (UAVs) must be able to navigate in a robust safe way, flying close to walls, the ceiling or the ground.

The analysis of the airflow rebound effects caused by nearby surfaces has been a subject of study for helicopters since the 1950s. Initially, the influence of the ground and its effect during low flights was studied. Also known as ground effect, it is a well-known phenomenon with frequent mentions in literature, while ceiling and wall effects are not as common. Ground effect was initially studied from a theoretical point of view based on the method of images by Cheeseman & Bennett [4]. This aerodynamic model represented the rotor of the helicopter and the ground as two sources of equal strength, causing the induced velocity at the rotor to be reduced in close vicinity to the ground. The model was later on compared to real single-rotor helicopter flights, stating that the theoretical approximation is acceptable for values of distance to the ground greater than 0.6 times the radius of the rotor and low values of aircraft speed. Since then, many experimental tests have been performed for both single-rotors [5, 6] and complete multi-copters [7–9], comparing real data to the theoretical model for helicopters. In [8] and [9], a test bench capable of measuring the thrust of the complete vehicle is used. In both cases, quadcopters are fixed to a force sensor and the ground surface is movable.

Ceiling effect is often studied as an analogous case to that of ground effect. Such is the case of [10], where the same setup as in [9] is used and the results are compared to

Extended author information available on the last page of the article

the ground effect model proposed by Cheeseman & Bennett. Also in [11], ceiling and ground effects are evaluated experimentally for both a single rotor and a quadrotor having as a reference the same Cheeseman & Bennett model. In [12] ground and ceiling effect experiments are conducted using a load cell and a static test bed. The results are validated with indoor flights and a VICON motion capture system. The results are applied to a surface-based optimal path planning algorithm that aims to reduce the thrust command when flying close to grounds and ceilings. Ceiling effect alone is frequently studied for bridge inspection [13–15], in which the experimental validation of the proposed models is also included. In [13], single-rotor and full quadcopter tests of ceiling effect are performed using the same test stand as in [8]. A mathematical model similar to the Cheeseman & Bennett's ground effect model is proposed. A custom UAV platform is later on designed to fly in contact with the ceiling and prove the advantages of this effect in terms of flight autonomy. In [14], the modelling and control design of a quadcopter are implemented for full contact bridge inspection missions. Authors in [15] address ceiling effect from a momentum theory point of view performing a later comparison to experimental results for a single rotor. In [16], an analysis on battery life is performed comparing UAVs flying close and away from the ceiling in time-fixed missions. Taking advantage of the thrust caused by the ceiling proximity, the use of the battery is reduced, extending the lifespan of the battery by 15.77%.

In [17–19] ground, ceiling and wall effects are experimentally evaluated. Conyers et al. [17] describe wall effect as a combination of a force and a pitching moment both towards the wall and independent from each other. Wall effect is evaluated using a fixed load cell and a quadcopter UAV in which the wall is positioned at different distances. Forces and torques are measured while simulating a hovering situation. In [20], a similar study is performed inside a climatic chamber in which the effect of pressure is considered in wall effect tests. In [18], the single-rotor and tandem rotor aircraft are studied for wall effect evaluation, taking into account only the total force measured in the perpendicular direction to the rotor plane. A single axis force sensor was used for this scope and the effect of the wall was considered negligible. Tests combining ground and wall effect were also performed. In [19], MEMS sensors are used for the measurement of pressure changes when flying near walls, ground and ceiling in order to characterize the differential pressure profiles when no distance measurement is available. Even if some research on the experimental evaluation of wall effect can be found in literature, most results are obtained from computational fluid dynamics (CFD) simulations [21–24].

This work is an extension of [25], in which additional experimental results are included. In the previous work, only results for wall effect were presented, considering three different levels of pressure and 8"x4.5" and 10"x4.7" propeller diameters. As a novelty in the present work, the analysis of ground and ceiling effects is included. Additional tests of wall effect are also performed while comparing two test setups at two independent facilities: terraXcube at EURAC Research and University of Denver.

The structure of this study is organized as follows. In Section 2, the setup and facilities are presented, the materials used to build the multicopter and the wall used for the experiments are described for each one of the facilities. The test methodology is assessed in Section 3, remarking the differences in the data collection processes and testing procedures. A description of the nondimensionalization process of forces and torques necessary to compare results obtained in different environmental conditions is provided in Section 4. A brief description of the measurement uncertainty evaluation process is given in Section 5. In Section 6, the most significant results are shown and commented, including comparisons amongst all the variations introduced in the tests and their uncertainty ranges. Eventually, in Section 7 the results are summarized and possible future development of the work is indicated.

2 Experimental Setup and Facilities

The test sessions take place at two different facilities: terraXcube, EURAC Research in Bolzano, in a large environmental chamber (LEC) and at the University of Denver (DU). The terraXcube LEC has a usable volume of 360 m^3 (12 m x 6 m x 5 m) that can simulate the most extreme environmental conditions on Earth's surface, allowing the synchronous control of multiple complex environmental parameters for long duration analyses.

In the University of Denver Unmanned Systems Research Institute (DU^2SRI) laboratory at the University of Denver, pressure and temperature have been logged at every test instance for later post-processing. The experiments conducted in this lab are subject to low pressure values due to the elevation of the city of Denver (1609 m above mean sea level).

In the field of multicopters, variations of climatic conditions are often employed to test harsh operation environments such as the ones encountered during search and rescue missions or exploration of deserted areas that could be hazardous for humans to explore. In [26, 27] and [28], experimental tests were conducted at terraXcube making use of the same force-torque sensor used in this work. The authors emphasize the lack of data points involving multicopter performance in extreme climatic conditions. For this reason, single-rotor tests were performed at different pressure and temperature levels to evaluate thrust and power amongst other parameters. In [27], a more complete study is presented including

full vehicle tests using a custom quadcopter. In [28] battery performance at different temperatures (from 25°C to -20°C) and altitudes (from 0 m to 5000 m) is analysed. The combinations of pressure and temperature parameters are chosen specifically to simulate a standard Alpine environment. In [29], higher altitudes (up to 9000 m) and different payloads (0-4 kg) are tested during free flight of a quadrotor inside the climatic chamber to asses the difficulties of planning a safe flight in a high altitude setting.

The evaluation of ground [9], ceiling [10] and wall effects [17] has been studied in previous works at the University of Denver. Tests were conducted for single propellers and a full vehicle for ground and ceiling effects using 9"x4.5" nylon propellers. A model for ground effect was obtained based on experimental data in [17], while the modelling of the remaining two effects was left as a future work.

In this work, the experimental assessment of wall effect was conducted in two different locations using part of the equipment used in previous publications by Conyers et al. [17] and Scanavino et al. [30]. In Section 2.1, a more detailed description of the material used in each facility is provided.

2.1 Equipment and Infrastructure

The first test sessions took place at terraXcube, a research facility, while the second test sessions were conducted at the University of Denver. In both cases, a quadcopter structure was fixed to a force-torque sensor attached to a heavy unmovable structure. Then, the various surfaces are placed nearby the test stand to evaluate the different phenomena. At University of Denver, only wall effect experiments were conducted. A description of the different testing equipment is provided hereafter.

2.1.1 Equipment at TerraXcube

The tests were conducted inside a climatic chamber with the possibility of controlling the pressure and temperature of the environment. For the experiments, these values have been kept constant at 20°C and 1000 hPa, respectively. The force-torque sensor used for these experiments is the JR3 30E15A4 [31], a 6 degrees of freedom (DOF) sensor with a capacity of ±200 N (F_x, F_y), ±400 N (F_z), ±16 N·m (T_x, T_y, T_z) and a resolution of 0.025 N (F_x, F_y), 0.05 N (F_z) and 0.002 N·m (T_x, T_y, T_z) with a stated accuracy of ±0.25% of all measurement ranges. All the measurements are acquired in digital mode using an Ethernet cable to connect the sensor to a board installed in the data collection computer. The test stand to which the sensor is attached consists on a tripod base structure with a hollow central cylinder that is filled with 25 kg of sand as in [27] to reduce mechanical vibrations. The cap on top of the cylinder is designed to fix the force-torque sensor. The propeller sizes tested in this facility were 10"x4.7" and 12"x5". Two UNI-T UT371 digital tachometers are placed at the base structure of the tripod that supports the sensor. This way, the rotation speed of two motors is logged directly into a PC thanks to their USB connector and software interface. The pulse-width modulation (PWM) signal sent to the Electronic Speed Controllers (ESCs) is generated by an Arduino UNO.

The quadcopter is constituted by four square aluminum arms that are fixed at the center of the structure. Individual motor supports are built and attached to each arm using pressure screws so that the positions of the motors can be changed if required. The distance between two non-consecutive motors is 500 mm, placing all motors at equal distances from each other forming an *'x'* configuration. Additionally, all motors lay at the same height. The UAV is powered using an APM SP-1U/2U Series power supply to avoid inconsistencies in voltage level encountered when using battery power sources. The APM power supply is capable of providing an adjustable level of voltage with a maximum of 800 V and a limit of 60 A.

The movable structure used to simulate the different surfaces can be seen in Fig. 1a and is composed by two main panels: 1) the ground or ceiling panel placed above the UAV and 2) the wall, found next to the tripod under the upper panel. Those two planes can be moved independently to be fixed at different distances with respect to the test stand. The upper surface acts as ground or as ceiling when the propellers are inverted or not, respectively. This surface has a reflective panel attached to it for the use of the tachometers.

2.1.2 Equipment at DU

The setup used for this experiments is constituted by a part of the setup used in [17], specifically the force-torque sensor, the quadcopter structure and the test stand tripod. The sensor is the ATI Mini40 [32] with the standard calibration US-20-40, which states a capacity of ±88.9 N (F_x, F_y), ±266.9 N (F_z), ±4.5 N·m (T_x, T_y, T_z) and a resolution of 0.022 N (F_x, F_y), 0.045 N (F_z) and 0.0006 N·m (T_x, T_y, T_z). The sensor is connected in a single-ended configuration to the National Instruments USB-6008 Digital Acquisition (DAQ) board that is connected to a PC. The tripod that holds the sensor has a hollow central cylinder filled with 20 kg of sand to reduce mechanical vibrations. The quadcopter frame is analogous to the one used previously at terraXcube but with a larger arm length of 44.5 cm. In this work, the speed of the motors is recorded using four SICK WLA16P photoelectric sensors [33] coupled with their own reflective surfaces placed over the test stand. These sensors are connected to an Arduino Mega 2560 Rev3 that is connected to the data collection computer. Also, an Arduino UNO is part of the setup as it controls the PWM signal sent to the ESCs.

(a) Test setup at terraXcube (b) Test setup at University of Denver

Fig. 1 Experimental setups found at the two testing facilities

The quadcopter is constituted by four square aluminum arms fixed at the center of the structure. Individual motor supports are built and attached to the extremes of the arms such that the distance between two non-consecutive motors is 890 mm. All motors are placed at equal distances from each other forming an *'x'* configuration. All motors lay at the same height.

The movable structure in this case is constituted by a plywood wall that is fixed to a wheeled base that facilitates the distance changes (Fig. 1b). A plywood square is positioned above the test stand with four identical reflectors for the photoelectric sensors. This square remains fixed as well as the test stand during all the experiments. The only movable part of the setup is the wall, that can be fixed by applying the brakes of the base wheels.

The quadcopter components and instrumentation can be found in Table 1 for both testing facilities.

3 Test Methodology

In this work, the experimental procedures used in the laboratories described above are very similar to each other. In both experimental sessions, fixed UAV tests are conducted, simulating an ideal hovering situation in which the surfaces are approached to the vehicle. An automatic PWM cycle is loaded and the data from the force-torque sensor is logged together with the tachometer and environmental data.

Each test has been conducted using a microcontroller that changes the PWM signal. This signal is sent to all ESCs in such a way that all motors receive the same input. Tests have been commanded with an ascending stair-shaped PWM signal whose complete cycle is repeated twice. Each step of the stair-shaped signal is kept constant for a sufficient amount of time to ensure that all signals reach a steady state.

Table 1 Setup characteristics

Parameter	Setup 1[a]	Setup 2[b]
Arm length	25 cm	44.5 cm
Tachometers	UNI-T UT371	SICK WLA16P
Power supply	APM SP-1U/2U Series	ARTESYN DS550-3
ESC	20 A	50 A
Motors	T-Motor 2212-18MN 920Kv	Leopard 2835-12T 690kv
Propeller 1	10"x4.7"	10"x4.5"
Propeller 2	12"x5"	12"x6"
Propeller 3		13"x6.5"

[a] Test setup used at terraXcube, EURAC Research Bolzano, Italy
[b] Test setup used at University of Denver, USA

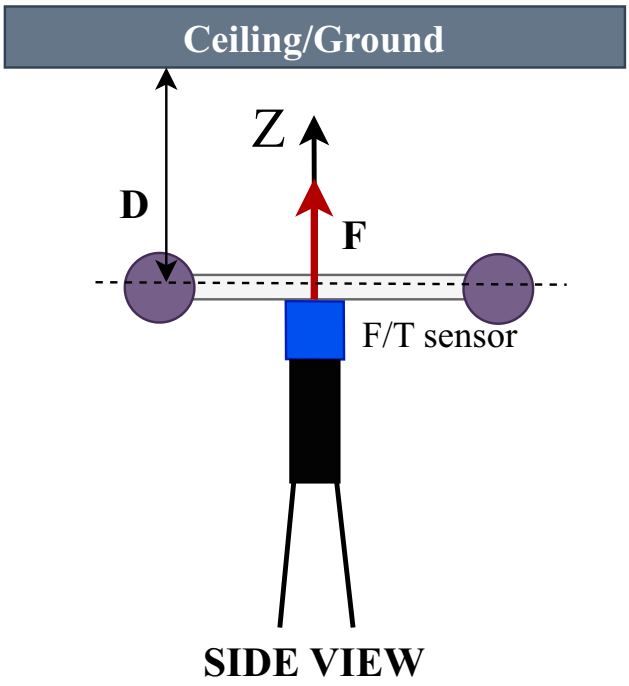

Fig. 2 Ground and ceiling effect axis and distance referencing

In this section as well as in Section 6, the symbols $F_{z\infty}$ and n_∞ are used to refer to the levels of total thrust and rotor speed placing the UAV far from any surface to avoid perturbations. The PWM values obtained for those force and speed levels are later on used for testing ground, ceiling and wall effects. Through this method, the authors intend to start from a known operation point from which the command is kept constant. This way, the changes in forces, torques and rotor speeds are due solely to the presence of disturbances.

3.1 Ground and Ceiling Effect Testing Methodology

For the evaluation of ground and ceiling effects all tests have been performed at terraXcube. The distances used for these experiments are: 5 cm, 15 cm, 25 cm, 35 cm and 100 cm and remain unchanged for both propeller sizes: 10”x4.7” and 12”x5”. They are measured as depicted in Fig. 2. Ground effect tests require the change of polarity of the ESCs and the inversion of the propellers. The surface used to emulate the ground is placed above the setup allowing it to remain almost unchanged and it is the same surface used for ceiling effect experiments.

PWM command values and duration can be seen in Fig. 3. For all experiments conducted at terraXcube, the panel place above the setup can be placed as far as 1 m distance. It is required for the placement of a reflective surface in order to obtain a reliable tachometer signal and cannot be placed any further.

The tests consist in ascending PWM levels that are repeated two times as it can be seen in Fig. 3. Each PWM level is maintained for 50 seconds and then switched to the next. In Table 2 each PWM value tested corresponds to a level of total thrust $F_{z\infty}$ and a level of average rotation speed of the rotors (n_∞).

The levels of $F_{z\infty}$ (total thrust) and n_∞ (average rotor speeds) used for comparison were chosen based on the limitations of each propeller. The maximum rotation speed achieved with 12”x6” propellers is 4000 RPM (*revolutions per minute*) and it will be lower than the one obtained with a propeller of a smaller size. The exact opposite is observed for thrust values, were the smaller propeller will reach a lower value (12.8 N). Once the maximum values and the respective halves are found and tested for forces and rotation speeds, the PWM mapping is complete.

3.2 Wall Effect Testing Methodology

To evaluate wall effect, different distances between the UAV and a wall must be tested. The distance to the wall is measured as a function of the radius of the propeller being used at each test. Such distance is often replaced by the relationship *D/R*, with *D* being the real distance to the wall and *R* the radius of the propeller. Distance is measured from the axis of the motors closest to the wall. This way, when we are aiming at a distance of one radius of the propeller (*1R*), we are placing the UAV as close to the wall as possible, preventing propellers from touching the wall by a distance of 1 mm $\pm$ 0.14 mm. It must be noted that even if the *D/R* ratio is equal, the real distance tested is not identical when using different propeller

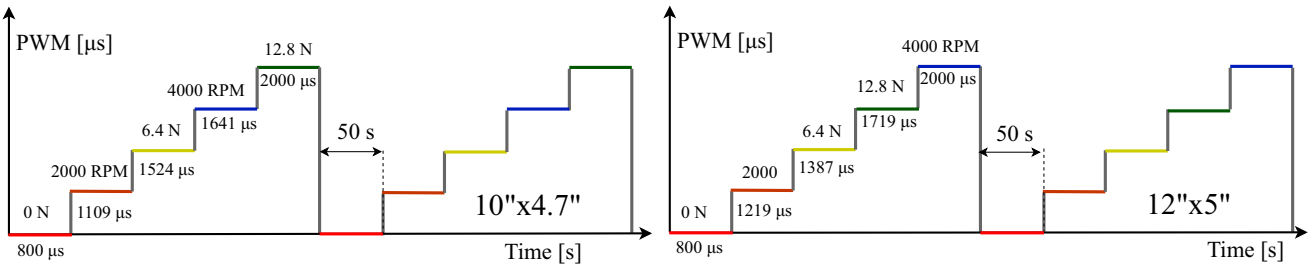

Fig. 3 PWM mapping for tests conducted at terraXcube

Table 2 PWM-$F_{z\infty}$-n_∞ mapping and testing parameters at terraXcube

Value	10"x4.7"				12"x5"			
PWM [μs]	1109	1524	1641	2000	1219	1387	1719	2000
$F_{z\infty}$ [N]	1.8	6.4	8.4	12.8	3.5	6.4	12.8	15.5
n_∞ [rev/min]	2000	3386	4000	4800	2000	2600	3700	4000
Ground/ceiling effect distances [cm]	5, 15, 25, 35, 100							
Wall effect distances [D/R]	1, 1.5, 2, 2.5, 3, ∼10							
F/T sensor	JR3 30E15A4							
Sampling rate [Hz]	10							
Duration of PWM level [s]	50							
Number of levels	4							

sizes. In this work, R_∞ is used to indicate a distance to the wall that is greater than ten times the radius of the propeller ($D \gg 10 \cdot R$). At such distance, the effect of the wall can be considered negligible [17].

The orientation of the UAV with respect to the wall can be seen for both cases in Fig. 4c. The axes disposition for each the JR3 and the ATI Mini40 sensors is also shown in Fig. 4a and b, respectively. The distance to the wall D is measured from the axes of the motors closest to it.

The orientation in which a one rotor is the closest to the wall has been overlooked in this work due to the small scale of the forces and torques to be measured. In such case, forces and torques would be smaller due to the action of only one rotor in proximity of the wall. The differences between the testing procedures at the two testing locations are described hereafter.

3.2.1 Test Methodology at TerraXcube

The tests conducted at terraXcube use the same F/T sensor as in [34]. The JR3 F/T sensor has a maximum sampling rate of 10 Hz using the digital data collection mode. The sixth filter available in the interface has been used for the reduction of noise in the logged data. Fourth order Butterworth filters are

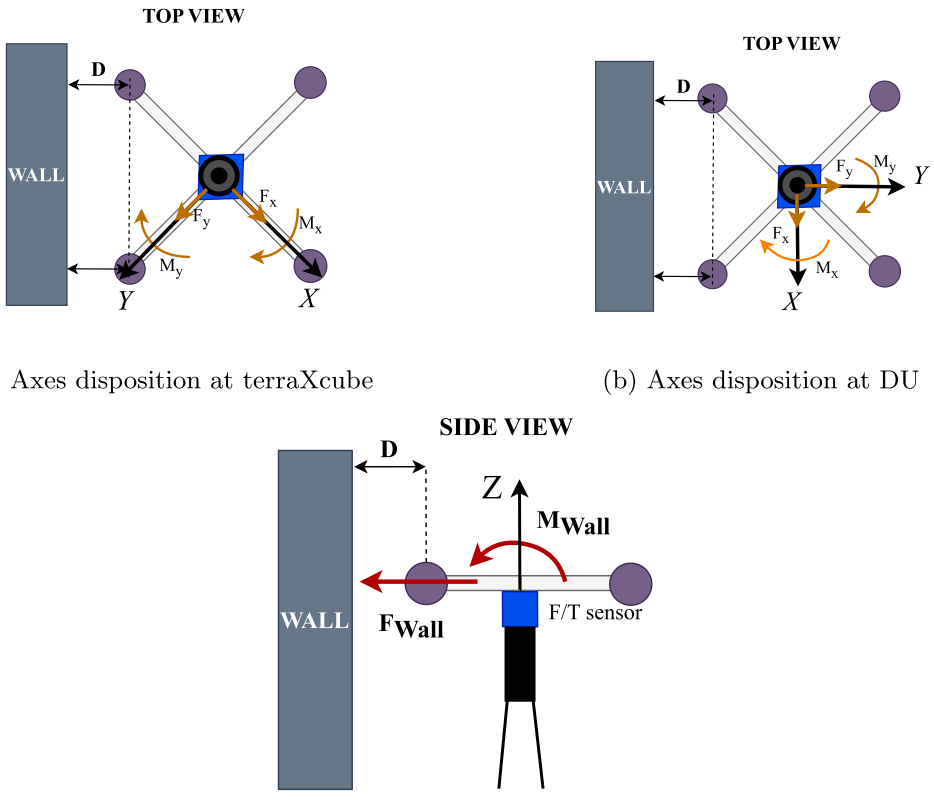

Fig. 4 Axes and orientation for wall effect experiments at the two testing facilities

(a) Axes disposition at terraXcube

(b) Axes disposition at DU

(c) Side view of wall effect experiments

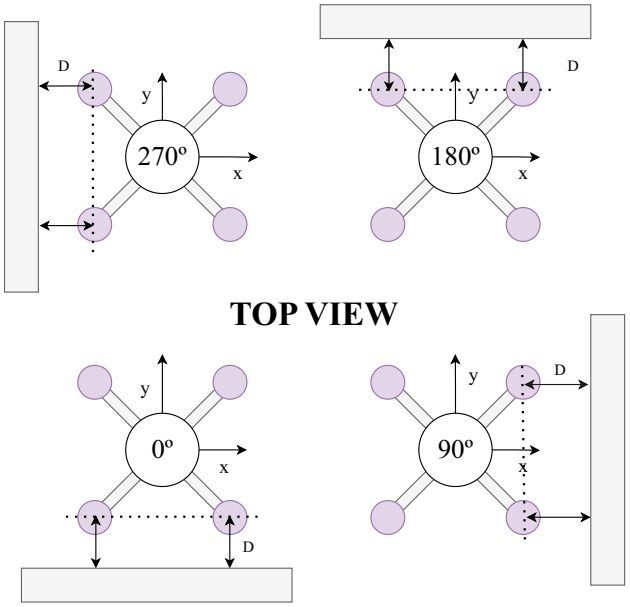

Fig. 5 Different testing orientations for wall effect evaluation at DU

implemented in the Analog to Digital converter (ADC) and can be selected from the interface. The data is directly used for post-processing without any further filtering. The tests have been conducted considering only one orientation of the setup (see Fig. 4a) and repeating each test twice. The first test is commonly discarded as it is usually performed with cold motors. The second test is considered for post-processing. The parameters for these test are the same as in the case of ground and ceiling effect evaluation and are reported in Table 2. Considering the orientation of the F/T sensor with respect to the wall, the forces and torques recorded by the load cell must be rotated during post-processing to obtain a single value for F_{Wall} and M_{Wall}. The results of the wall effect experiments conducted in this facility presented in this work comprise only 10"x4.7" and 12"x5" propellers. The use of smaller propellers has been discarded in the present work.

It was established in [20] and [25] that smaller propellers produce low values of forces and torques in wall effect tests that are challenging to capture with the available setup. The distances tested for wall effect evaluation in this facility are the following: 1 R, 1.5 R, 2 R, 2.5 R, 3 R and R_∞.

3.2.2 Test Methodology at DU

An ad-hoc software has been created for the data logging of the ATI Mini40 F/T sensor. The use of the NI-USB-6008 DAQ to transform the analog data coming out of the sensor allows the user to achieve a faster sample rate than in the case of the JR3 sensor. A sample rate of 150 Hz was used and the raw data is filtered during post-processing, not during testing. A fifth order Butterworth filter is used for this purpose.

Only wall effect tests were conducted in this facility, also using different distances from the ones in previous tests. The tests consist in two cycles of ascending PWM values that stay constant for 15 seconds each. As in [17], the wall is placed on the four orientations with respect to the UAV as reported in Fig. 5. Then, each distance and orientation is tested five times. The average between all four orientations is obtained to eliminate possible setup imbalances or sensor coupling effects.

The thrust and rotation speed levels that have been tested in this facility are the following: 8 N, 10 N, 12 N, 14 N and 3000 RPM. The propeller dimensions tested are 10"x4.5", 12"x6" and 13"x6.5". In Table 3, the PWM mapping for these tests can be seen. As stated before, each PWM value tested corresponds to a level of total thrust $F_{z\infty}$ and a level of average rotation speed of the rotors. These values are obtained previously to actual tests, placing the UAV far from any surface. Then, the PWM commands found through this process are used for all tests.

A schematic of the test structure is presented in Fig. 6.

Table 3 PWM-$F_{z\infty}$-n_∞ mapping and testing parameters at DU

Value	10"x4.5"					12"x6"					13"x6.5"				
PWM [μs]	1371	1500	1570	1632	1676	1430	1529	1586	1636	1681	1441	1478	1513	1520	1544
$F_{z\infty}$ [N]	4.3	8	10	12	14	5.5	8	10	12	14	8	10	12	12.5	14
n_∞ [rev/min]	3000	4000	4400	4800	5200	3000	3600	4000	4400	4700	2500	2800	3000	3100	3250
Wall effect distances [D/R]	1, 1.25, 1.5, 1.75, 2, 2.5, 3, ∼ 10														
F/T sensor	ATI Mini40														
Sampling rate [Hz]	150														
Duration of PWM level [s]	15														
Number of levels	5														

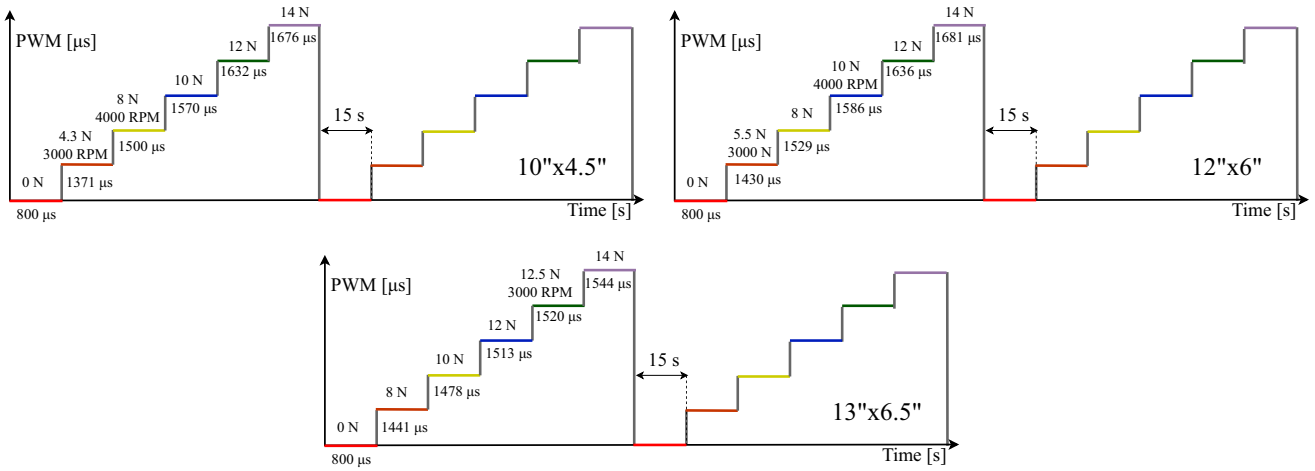

Fig. 6 PWM mapping for tests conducted at DU

4 Data Reduction

For the comparison of test data collected at different facilities and environmental conditions, the reduction or nondimensionalization of the data is required. For this purpose, the following expressions are used [27]:

$$c_T = \frac{F_z}{0.5\rho n^2 d^4} \tag{1}$$

$$c_F = \frac{F_{Wall}}{0.5\rho n^2 d^4} \tag{2}$$

$$c_Q = \frac{M_{Wall}}{0.5\rho n^2 d^5} \tag{3}$$

where c_F, c_T and c_Q are the force, thrust and torque coefficients, respectively. F_{Wall} and M_{Wall} are the force and torque values in the direction of the wall, F_z is the thrust force of the complete UAV, ρ is the air density computed using the ideal gas law Eq. 5, n is the average of the rotor speeds [rev/s] and d is the propeller diameter. Data reduction is considered for all tests for an easier comparison between propeller diameters and pressure differences.

5 Measurement Uncertainty

In this section, the evaluation of the uncertainty of the measurements present in this work is introduced. The analysis is based on the *Guide to the expression of uncertainty in measurement* (GUM) [35] and all uncertainty ranges in this manuscript are indicated for a 95% confidence interval (k=2). In the text, numerical values reference the relative expanded uncertainty (REU), computed as in Eq. 4, where $U(x_i)$ is the combined expanded uncertainty and $|x_i|$ is the absolute value of the measurement. First, an analysis of each F/T sensor together with their available uncertainty information is provided. Then, the formulation to obtain uncertainty values for forces and torques is explained. Finally, the dimensionless coefficient uncertainty is addressed. Refer to the supplementary information (SI) material [36] for a detailed description of the measurement uncertainty evaluation.

$$REU = \frac{U(x_i)}{|x_i|} \ni |x_i| \neq 0 \tag{4}$$

For values of $|x_i|$ very close to 0, instead of the REU the expanded uncertainty is reported.

6 Results

In this section, the results obtained during the experimental tests are summarized and presented. Initially, the results from each one of the effects are presented individually in the following order: ground effect, ceiling effect, wall effect.

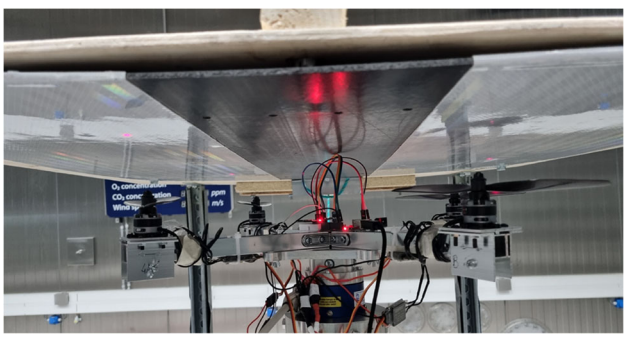

Fig. 7 Ground effect setup layout

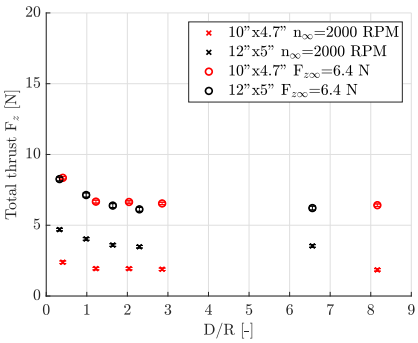

(a) Results at PMW levels between 1100 μs and 1600 μs for 10”x4.7” (red markers) and 12”x5” (black markers) propellers

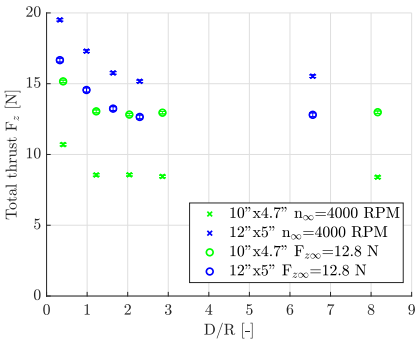

(b) Results at PMW levels between 1600 μs and 2000 μs for 10”x4.7” (green markers) and 12”x5” (blue markers) propellers

Fig. 8 Ground effect results for 10”x4.7” and 12”x5” propellers. Circles refer to the total thrust obtained when giving the PWM command obtained for $F_{z\infty}$. Crosses indicate the thrust achieved for the PWM command obtained for n_∞

The results are also shown considering the temperature and pressure variations of the environment by the computation of the corresponding force and torque coefficients including the corresponding uncertainty ranges. Then, the effect of the air density on the total thrust of the quadcopter is analyzed comparing the data collected in the various facilities for wall effect experiments. Also, the distance to the wall is compared to the thrust of the full quadcopter.

Constant values of total vehicle thrust $F_{z\infty}$ and n_∞ for all the motors are set throughout the tests in order to facilitate the comparison between them. Such levels are described in Tables 2 and 3 for the tests conducted at terraXcube and DU, respectively.

The data obtained for the evaluation of ground, ceiling and wall effects is available at the SI repository.

6.1 Ground Effect

The horizontal surface is placed above the multicopter, which propellers have been inverted together with the motor polarity. Each propeller is flipped and two cables connecting each ESC to each motor are swapped, changing the direction of rotation of the motors. This ensures that the rotation of the motors is in accordance with the propeller direction of rotation. The airflow is consequently directed upwards, causing the surface to act as ground. The thrust component is measured as a negative force by the F/T sensor. All values of forces have been converted to positive values during post-processing for convenience. In Fig. 7, the test layout for ground effect experiments is shown.

The distances tested are the following: 5 cm, 15 cm, 25 cm, 35 cm and 100 cm. No variations in temperature and

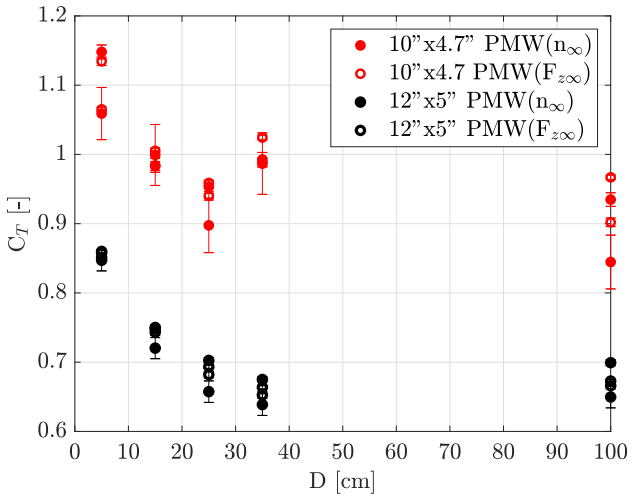

Fig. 9 Ground effect thrust coefficients at different levels of PWM for $F_{z\infty}$ and n_∞. Hollow circles refer to the coefficient values obtained when giving the PWM command obtained for $F_{z\infty}$. Full circles indicate the coefficients achieved for the PWM command obtained for n_∞

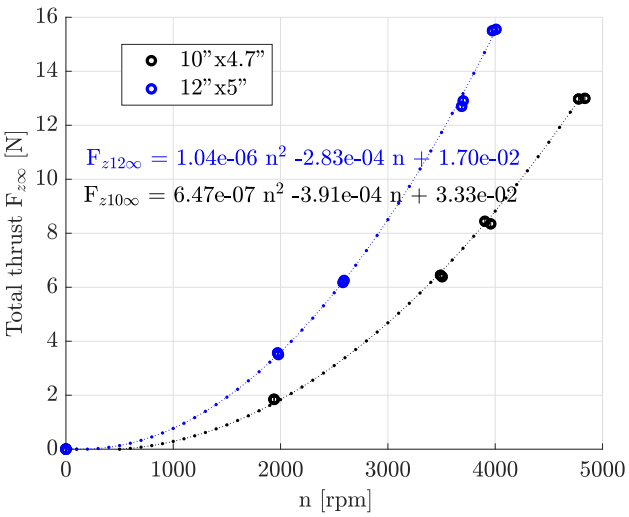

Fig. 10 Relationship between total thrust *OGE* and rotational speed of the motors

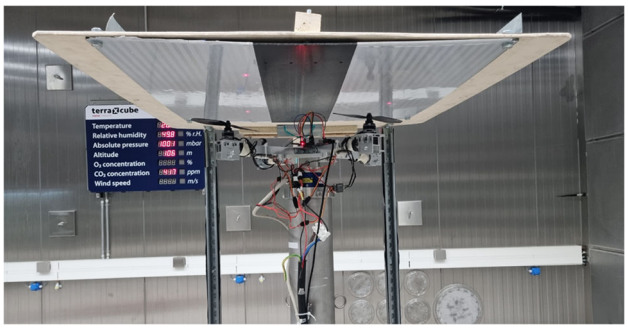

Fig. 11 Ceiling effect setup layout

pressure were defined during these tests, remaining constant around 20°C and 1000 hPa.

In Fig. 8, the result of the tests for 10”x4.7” and 12”x5” propellers are shown. A UAV is considered out-of-ground effect (*OGE*) when the distance from the rotor plane to the ground has no effect on the total thrust of the vehicle. In these experiments a value of $D > 6R$ has been considered OGE due to setup constraints.

In Fig. 8a, points obtained with the PWM corresponding to n_∞=2000 RPM and $F_{z\infty} = 6.4$ N are shown. As expected at equal values of n_∞, the two propeller sizes produce different levels of total thrust *OGE*. At equal thrust levels ($F_{z\infty}$), both propellers increase the total thrust of the vehicle by a value close to 2 N when placed at 5 cm to the ground. On the case of command based on n_∞, a lower gain is obtained. Uncertainty error bars are not significantly visible due to the wide range of forces displayed. Uncertainty values range from 1.25% up to 3.9% depending on the operation point.

The cases with a command corresponding to n_∞ = 4000 RPM and $F_{z\infty}$ = 12.8 N are shown in Fig. 8b. The n_∞ = 4000 RPM results indicate and increase in thrust of 2.3 N in the case of the 10”x4.7” propellers and an increase of near 5 N in the 12”x5” case. The $F_{z\infty}$ = 12.8 N tests produce a increase of 2.3 N for the 10”x4.7” propellers and 3.8 N for the 12”x5” propellers. As expected, a bigger propeller diameter produces a greater increase in thrust as a higher volume of airflow is being pushed against the ground. Uncertainty values remain in the range of 0.5% and 0.9%.

In [9], ground effect on full quadcopters is different from the single propeller effect by a detrimental thrust performance in the area $1.5R < D < 2R$. After this zone, an increase in thrust is produced that lasts until $D \approx 9R$. In the present work, such tendency is not clearly observed due to the lack of datapoints in the zone $3R < D < 6R$. More tests must be conducted to completely characterize this phenomenon.

In Fig. 9, the force and torque coefficients corresponding to the datapoints in Fig. 8 are presented considering the real distances to the ground and the uncertainty ranges based on each operation point. As it was expected, the value of c_T characterizes the behavior of each propeller regardless of the different values of PWM. This result can be explained by analyzing the relationship between F_z and n, since the rest of the parameters in Eq. 1 remain close to constant during these experiments. The uncertainty ranges are strongly dependant on the coefficient formula and variables. Uncertainty values range from 0.4% to 4.6%.

The relationship between total thrust and rotor speed can be seen in Fig. 10, where a parabolic tendency is observed ($F_z \sim n^2$). Two points are found at each RPM value which correspond to the two measurements of the F/T sensor at that propeller speed that are obtained by repeating the PWM stair command twice per test (see Fig. 3). The results in Fig. 9 are in accordance with this relationship since the ratio F_z/n^2 remains nearly constant for each propeller type. No uncertainty ranges have been included in Fig. 10 as they are considered negligible in the ranges depicted.

6.2 Ceiling Effect

A ceiling is simulated by placing a 1 m^2 surface above the test bed. The propellers are installed in the regular position,

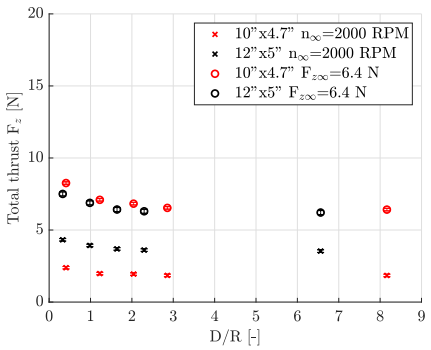

(a) Results at PMW levels between 1100 μs and 1600 μs for 10”x4.7” (red markers) and 12”x5” (black markers) propellers

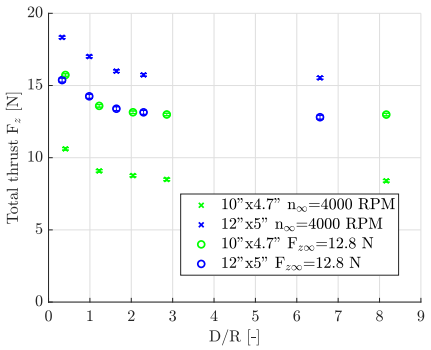

(b) Results at PMW levels between 1600 μs and 2000 μs for 10”x4.7” (green markers) and 12”x5” (blue markers) propellers

Fig. 12 Ceiling effect results for 10”x4.7” and 12”x5” propellers. Circles refer to the total thrust obtained when giving the PWM command obtained for $F_{z\infty}$. Crosses indicate the thrust achieved for the PWM command obtained for n_∞

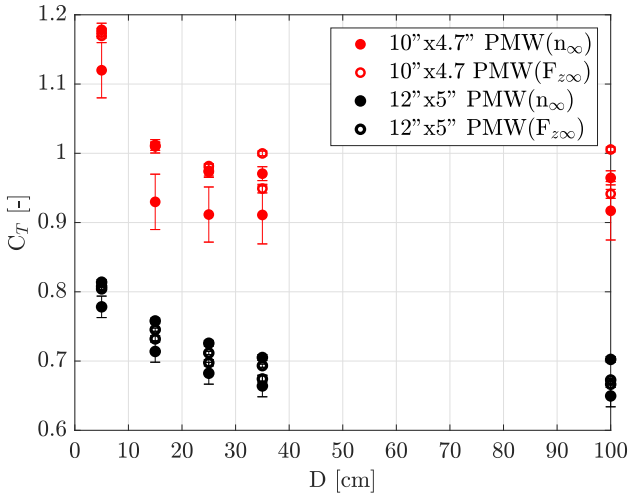

Fig. 13 Ceiling thrust coefficients at different levels of PWM for $F_{z\infty}$ and n_∞. Hollow circles refer to the coefficient values obtained when giving the PWM command obtained for $F_{z\infty}$. Full circles indicate the coefficients achieved for the PWM command obtained for n_∞

directing the airflow downwards. In Fig. 11, the setup for these experiments can be seen.

Testing the same levels of thrust and RPM as in the ground effect case, the results obtained are displayed in Fig. 12.

The increase of thrust in the case of ceiling effect is less significant than in the case of ground effect. In Fig. 12a, the greatest increase in thrust is obtained for the 10”x4.7” propellers in the fixed thrust case with an extra 1.85 N. For $F_{z\infty}$=12.8 N, the smaller propellers obtain a difference of 2.7 N and the bigger propellers 2.5 N. At n_∞=4000 RPM, small and big propellers obtain a gain of 2.2 N and 2.7 N, respectively. A value of $D > 6R$ is considered out-of-wall effect (*OWE*) in this work. As for ground effect force results, uncertainty error bars are not significantly visible due to the wide range of forces displayed. Uncertainty values range from a 0.5% up to a 3.9% depending on the operation point for both Fig. 12a and b.

The dimensionless coefficients corresponding to the results in Fig. 12 are shown in Fig. 13.

A similar behavior as for ground effect is presented for ceiling effect thrust coefficients, where uncertainty values range from a 0.4% to a 4.6%.

As expected, coefficients from ground and ceiling effect tests are found in the same range, with 12”x5” coefficients being lower in the ceiling effect case due to the lower thrust gain obtained in this case. As it can be seen in Fig. 14, as the UAV gets closer to a horizontal surface, the total thrust increases. This can be confirmed by the results obtained for both ground and ceiling effect tests. The curve that describes the relationship between rotor speed and total thrust becomes steeper as the UAV approaches the ground or ceiling. No direct conclusion can be obtained about the variations in rotor speed as distance to both surfaces is reduced.

6.3 Wall Effect

Wall effect has been tested in the two experimental facilities presented in Section 2.1. The results are first analyzed separately, then a comparison is made in terms of total thrust of the vehicle to assess the effect of air density, propeller type and influence of the wall in the total thrust of the quadcopter. Uncertainties are reported as expanded uncertainty values instead of relative expanded uncertainties due to the values of the coefficients having values very close to 0, causing the relative uncertainty to lose its purpose.

6.3.1 Wall Effect Tests at TerraXcube

Preceded by the results from [20] and [25], bigger propellers have been tested as a consequence of the scarce information obtained with propellers with $d \leq 9$”. In this case, the two propeller sizes used are: 10”x4.7” and 12”x5”. The setup used can be seen in Fig. 1a.

In Fig. 15, the torque and force coefficients for 12”x5” propellers can be seen. Figure 15a, the comparison in terms

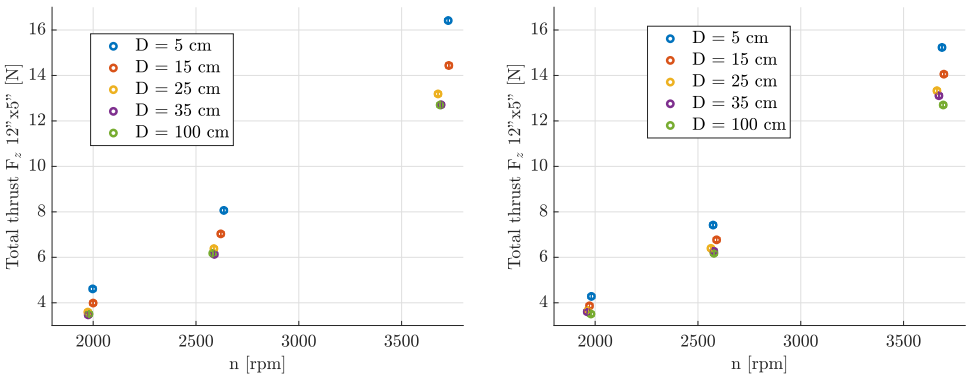

(a) Ground effect tests (b) Ceiling effect tests

Fig. 14 Relationship between motor speed and total thrust of the UAV in and out of ground and ceiling effects for 12”x5” propellers

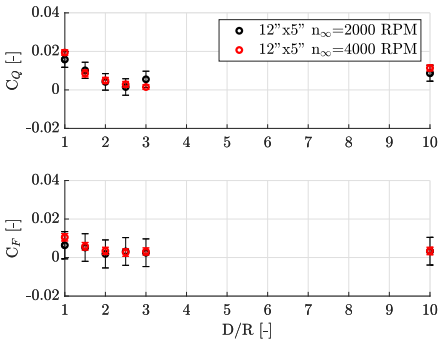

(a) Force and torque coefficients at n_∞=2000 RPM (black circles) and n_∞=4000 RPM (red circles)

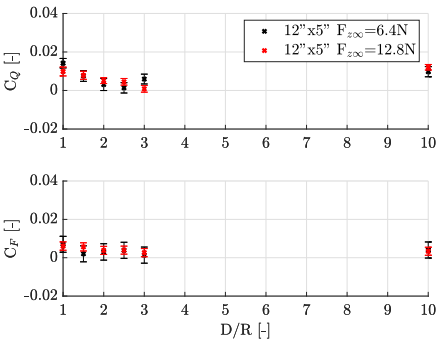

(b) Force and torque coefficients at $F_{z\infty}$=6.4 N (black crosses) and $F_{z\infty}$=12.8 N (red crosses)

Fig. 15 Wall effect results for 12"x5" propellers. Crosses refer to the coefficient values obtained when giving the PWM command obtained for $F_{z\infty}$. Circles indicate the coefficients achieved for the PWM command obtained for n_∞

of RPM levels is made. In Fig. 15b, the comparison in terms of total thrust is displayed.

The coefficients at $D = 10$ R are non zero due to the fact that only one orientation has been tested in terraXcube. The values of force and torque are therefore non zero and can be affected by the uncertainty of the sensor and additional noise components.

Nevertheless, an increasing pattern is detected when the distance to the wall is reduced. The force coefficients remain in the range between 0 and 0.01, while the torque coefficients reach a value of 0.018 in the n_∞=4000 RPM case.

The uncertainty value in Fig. 15a are around ±0.002 for c_Q whereas for c_F, the minimum uncertainty value is ±0.002 and the maximum reaches ±0.007. For Fig. 15b uncertainties have a minimum of ± 0.001 and a maximum of ± 0.002 for c_Q values whereas for c_F, the minimum is ± 0.002 and the maximum reaches ± 0.004.

In Fig. 16, the results for 10"x4.7" propellers are shown. The uncertainty ranges for the lower rotation speed coefficients for both propeller sizes are wider than for the other cases. This is due to the definition of the coefficients, in which the value of the n or rotation speed has a great weight, which becomes amplified in the expression of the uncertainties. In Fig. 16a, the c_Q has a maximum uncertainty of ± 0.01 and a minimum uncertainty of ± 0.004. For c_F, those values increase reaching a maximum of ± 0.02 and minimum of ± 0.005. In Fig. 16b, c_Q goes from ± 0.003 to ± 0.005 and c_F from ± 0.003 to ± 0.006.

In future experiments, all orientations will be tested and the averaging of the data will provide clearer results with lower uncertainty levels.

6.3.2 Wall Effect Tests at DU

Three different propeller diameters are tested in a robotics laboratory, where the pressure and temperature remain at levels around 23°C and 800 hPa.

In [17], the wall structure was placed on the four sides of the setup and the average between such tests was conducted in order to eliminate imbalances and other bias factors. In the tests conducted at DU in the present work the same procedure has been followed, in which all four orientations have been tested. Additionally, each test is repeated five times. Four of them are averaged to further increase steadiness and reduce noise.

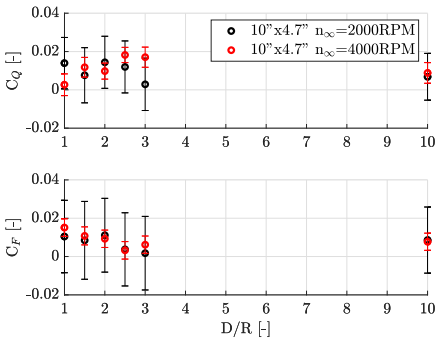

(a) Force and torque coefficients at n_∞=2000 RPM (black circles) and n_∞=4000 RPM (red circles)

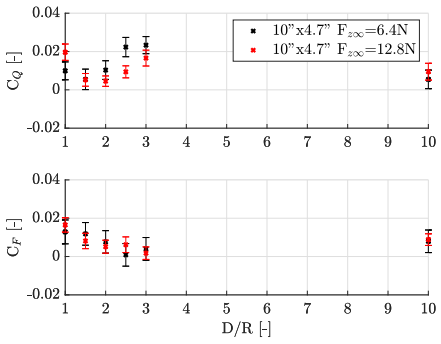

(b) Force and torque coefficients at $F_{z\infty}$=6.4 N (black crosses) and $F_{z\infty}$=12.8 N (red crosses)

Fig. 16 Wall effect results for 10"x4.7" propellers. Crosses refer to the coefficient values obtained when giving the PWM command obtained for $F_{z\infty}$. Circles indicate the coefficients achieved for the PWM command obtained for n_∞

In Fig. 17, the torques obtained for the three propeller sizes tested are shown. As it can be appreciated for 10”x4.5” and 12”x6” propellers, the torque increases as the total thrust of the vehicle is raised. When approaching the wall the torque increases reaching values of around 0.05 N·m.

The resolution values for forces and torques for the ATI Mini40 are 0.022 N and 0.0006 N·m, respectively. In this case, the torques measured are two orders of magnitude above the corresponding resolution limit. The uncertainty bars remain at a value of ± 0.056 N·m, staying very close to the manufacturer stated uncertainty. This indicates that the most relevant uncertainty component for these measurements is not the measure unsteadiness but the stated type B uncertainty from the calibration certificate.

In Fig. 18, the force and torque coefficients for the 10”x4.5”, 12”x6” and 13”x6.5” propellers are shown. Such coefficients have been obtained by averaging the force and thrust coefficients of all levels presented in Fig. 17.

The coefficients obtained remain very close to each other, suggesting a growing tendency when reducing the distance to the wall. The uncertainty ranges of c_Q are minimum for 12”x6” propellers with a value of ± 0.005. The maximum value is found for 10”x4.5” at ± 0.01. For c_F, the minimum uncertainty is ± 0.03 for 12”x6” and the maximum is ± 0.06 for 10”x4.5” propellers. The uncertainty ranges for c_F also indicate that with such small coefficient values, any apparent tendency is not reliable. The axes scaling is left constant for all wall effect coefficients for an easier comparison.

The resolution of the JR3 sensor for the torques is 0.002 N·m, while the resolution for forces in the x and y axes is 0.025 N. The ATI Mini40 sensor has a resolution of 0.022 N for F_x and F_y, while M_x and M_y have a resolution of 0.0006. In [23], the CFD evaluation of wall effect for a 15”x5.5” propeller quadcopter was performed obtaining maximum values of forces and torques of 0.098 N and 0.075 N·m, respectively, at a distance of 1.2 R from the wall. Using these results as a reference for experimental tests, wall effect forces for smaller quadcopters would have values very close or under the resolution limit of both sensors. While both sensors should be capable of measuring the torques present in wall effect experiments in terms of resolution, the stated uncertainty of the ATI Mini40 has a value of ±0.06 N·m, which represents a REU of 80% for a torque of 0.075 N·m. The computed expanded uncertainty of the JR3 sensor for x and y values of torques has a value of ±0.003, translating to a REU of 3.6%. The choice of sensors must be made considering resolution and uncertainty values of the force/torque sensors. Because a complete uncertainty evaluation of the ATI Mini40 sensor has not been performed, its suitability for wall effect experiments has been proven to be poor based on the datasheet information and comparison to CFD results. On the other hand, thanks to the uncertainty evaluation performed for the

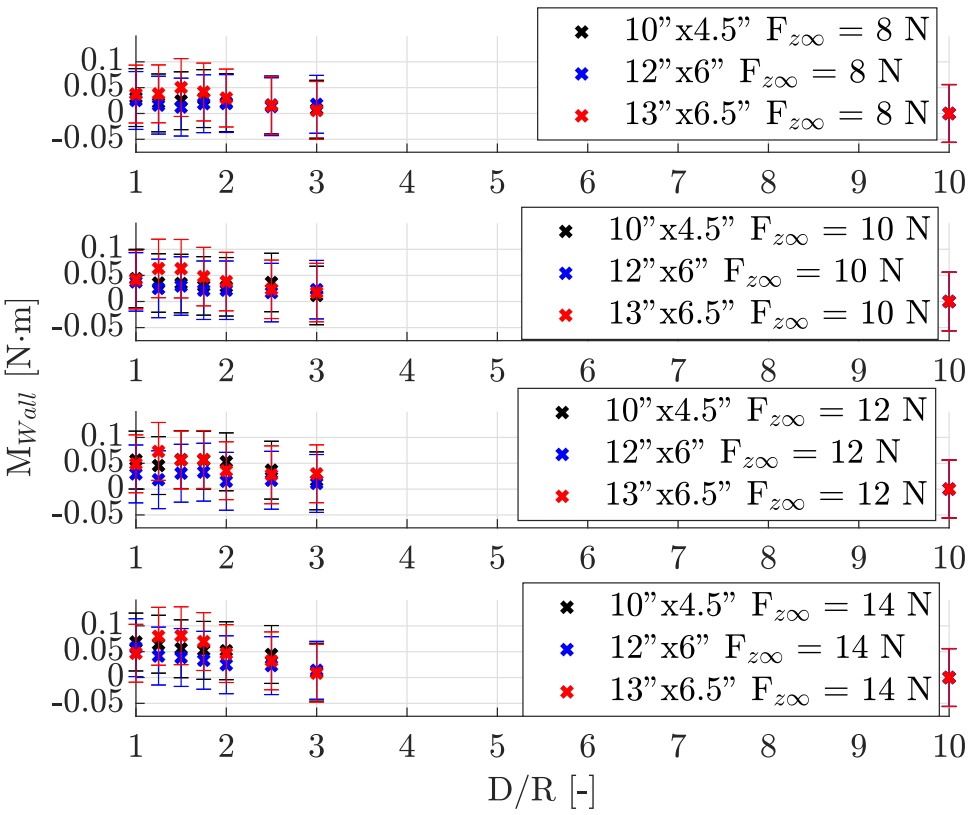

Fig. 17 Torque values for 10”x4.7”, 12”x6” and 13”x6.5” propellers at different levels of PWM obtained at F$_{z\infty}$ obtained at DU

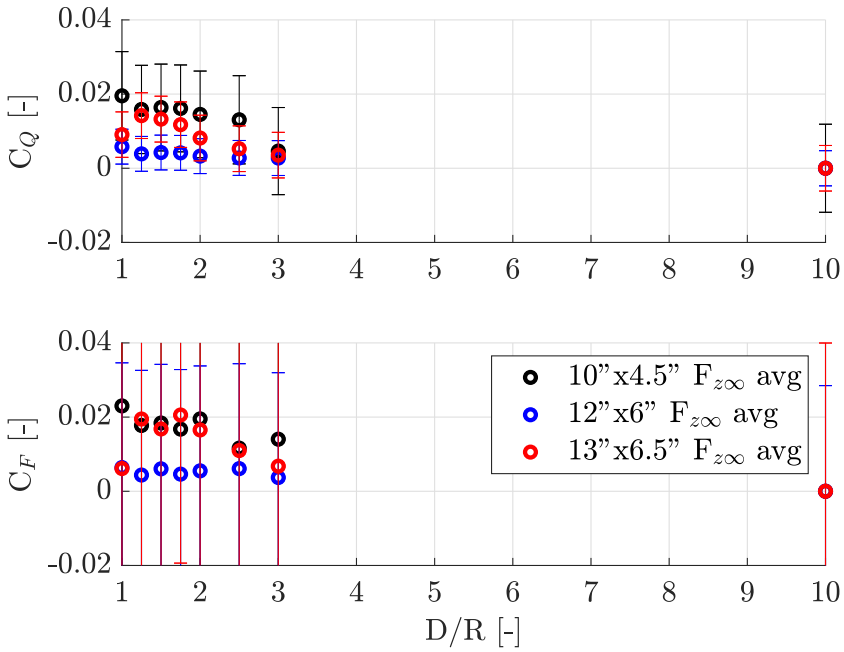

Fig. 18 Wall effect results for 10”x4.5” (black markers), 12”x6” (blue markers) and 13”x6.5” (red markers) propellers at DU. Force and torque coefficients average of all levels of equal $F_{z\infty}$

JR3 sensor, the JR3 sensor appears to be a more adequate option for such tests.

6.4 Total Thrust in Wall Effect Conditions

In this section, the impact on total thrust of the UAV during near-wall flights is analysed. Using Eq. 1, the thrust coefficients can be obtained for the same test data gathered during wall effect experiments.

The tests are conducted at ambient conditions in both facilities, being 20°C and 1000 hPa for terraXcube and 23°C and 800 hPa for DU. The differences in temperature are almost negligible, while the pressure has an important contribution in the air density of each location. Following the Ideal Gas Law in Eq. 5:

$$P = \rho R T \tag{5}$$

Where P is the pressure value, ρ is the air density, R is the molar gas constant and T is the temperature. The approximate densities obtained are 0.98 kg/m^3 and 1.17 kg/m^3 for DU and terraXcube, respectively.

In Fig. 19 , thrust coefficients corresponding to all wall effect tests are presented with respect to the air density and distance to the wall. In Fig. 19a, the thrust coefficients c_T are shown with respect to the ratio $\frac{\rho}{\rho_{DU}}$, where ρ_{DU} is the density value at the University of Denver. Pink dots represent the average of the data points belonging to each point cluster in Fig. 19a. Given the differences in pitch from the propellers tested in the different locations, a direct comparison of the coefficient values cannot be made. However, lower pitch propellers obtain higher values of c_T. In Fig. 19b, the relationship between all thrust coefficients and the coefficients obtained away from the wall is shown with respect to the distance of each test. All markers remain close to a ratio value of 1, except for the 10”x4.7” propellers tested at ter-

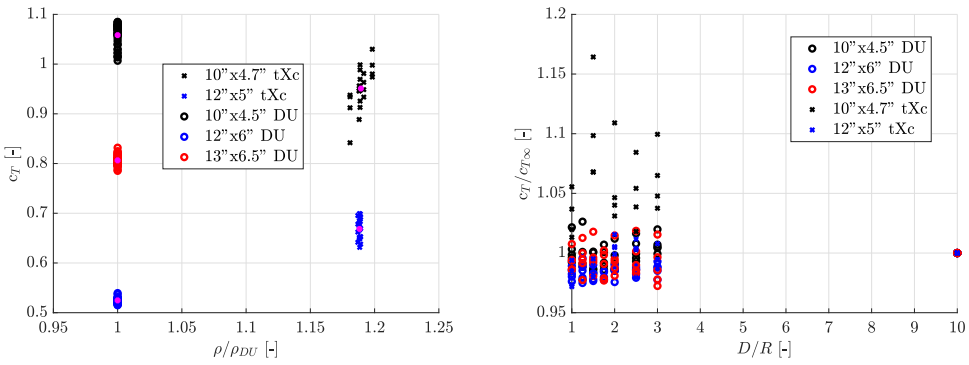

(a) Thrust coefficient c_T (b) Ratio between c_T and $c_{T\infty}$

Fig. 19 Total thrust coefficients for all wall effect tests. Crosses denote tests conducted at terraXcube and circles are those performed at DU

raXcube that display a noisier behavior also noted in all the results presented in the previous sections. The uncertainties of the coefficient ratios obtained at terraXcube have a value between a 0.9% and a 6.4% and are discrete compared to the relative uncertainties for the DU data in which the values go from a 33.5% up to a 108.5% relative to the ratio value. The uncertainty levels for the ATI Mini40 sensor indicate that no reliable conclusions can be obtained for DU tests. On the other hand, the results obtained with the JR3 present a lower uncertainty and therefore can be trusted on the fact that no significant effect of the wall on the total trust of the quadcopter is detected. This result is reached assuming that the speed of the motors suffer no great variations during wall effect tests, ensuring that F_z is the only parameter changing in the c_T expression. Then, one can conclude that the effect of the wall has a negligible impact on the total thrust of the UAV.

As predicted in [18], the effect of the wall on the total thrust of the vehicle can be considered negligible.

7 Conclusions

An experimental evaluation of ground, ceiling and wall effects for quadcopters has been performed taking into account different testing parameters such as propeller size, pressure levels and PWM commands. Ground and ceiling effect experiments have confirmed the thrust gain caused by the airflow rebound and suction, respectively. Ground effect produces a greater increase in thrust than ceiling effect. In both cases, a seemingly growing exponential tendency of the total thrust of the vehicle is noticed when approaching the respective surfaces. Thrust coefficients characterize each propeller type tested, reaching the same values for different levels of rotor speed and total thrust. Additionally, the rotor speed is influenced by the presence of surfaces, decreasing in the proximity of ceilings and increasing in the proximity of the ground. In the case of wall effect, the distance to the wall induces a pitching moment towards the wall with an apparent exponential tendency. A similar situation is found for the forces towards the wall, which grow when the distance is reduced. The forces and torques measured in these experiments have proven to be small and difficult to measure with the sensors available. A thorough measurement uncertainty analysis has been performed in order to provide a reliability level to the data presented. The decrease of the air pressure influences the vertical thrust and also the forces and torques acting on a UAV when flying in wall, ground or ceiling effect, making the experimental evaluation of these effects an even greater challenge. This work aims to partially fill the experimental gap existing in the literature regarding the evaluation of ground, ceiling and wall effect in different pressure conditions, approaching these phenomena from a more exhaustive perspective including variations in propeller type and other testing instrumentation. The novelty of the work is not only the comparison of setups and instrumentation but also the careful measurement of test parameters such as temperature, pressure and rotation speed of the motors, which are commonly assumed constant or estimated, respectively. Also, the availability of the data and the uncertainty evaluation give additional weight to the results presented in this manuscript.

The data obtained can be used for the development of simulation models and design of control and navigation algorithms that involve near-wall flights. All datasets together with the measurement uncertainty evaluation can be found in the Supplementary information repository in [36].

Supplementary Information The online version contains supplementary material available at https://doi.org/10.1007/s10846-024-02155-7.

Acknowledgements The authors would like to thank Andrea Eccher and the rest of terraXcube Eurac Research staff for their support and collaboration during test activities. We also thank Prof. Gonçalo Fernandes Pereira Martins and the people at the University of Denver Unmanned Systems Research Institute, who helped on the construction of the new setup.

Author Contributions
- Conceptualization: Iris David Du Mutel de Pierrepont Franzetti, Riccardo Parin, Elisa Capello, Matthew J. Rutherford, Kimon Valavanis
- Methodology: Iris David Du Mutel de Pierrepont Franzetti, Riccardo Parin, Elisa Capello, Matthew J. Rutherford
- Formal analysis and investigation: Iris David Du Mutel de Pierrepont Franzetti
- Writing - original draft preparation: Iris David Du Mutel de Pierrepont Franzetti
- Writing - review and editing: Riccardo Parin, Elisa Capello, Matthew J. Rutherford, Kimon Valavanis
- Funding acquisition: Riccardo Parin, Elisa Capello
- Resources: Riccardo Parin, Elisa Capello, Matthew J. Rutherford, Kimon Valavanis
- Supervision: Riccardo Parin, Elisa Capello, Matthew J. Rutherford, Kimon Valavanis

Funding Open access funding provided by Politecnico di Torino within the CRUI-CARE Agreement. The PhD scholarship is funded by Eurac Research Bolzano

Data Availability Not applicable

Declarations

Competing Interests The authors have no relevant financial or non-financial interests to disclose

Ethics approval Not applicable

Consent to participate Not applicable

Consent to publish Not applicable

References

1. Boonyathanmig, N., Gongmanee, S., Kayunyeam, P., Wutticho, P., Prongnuch, S.: Design and implementation of mini-uav for indoor surveillance. Proceeding of the 2021 9th International Electrical Engineering Congress, iEECON 2021, 305–308 (2021). https://doi.org/10.1109/IEECON51072.2021.9440350
2. Harik, E.H.C., Guerin, F., Guinand, F., Brethe, J.F., Pelvillain, H.: Towards an autonomous warehouse inventory scheme. 2016 IEEE Symposium Series on Computational Intelligence, SSCI (2016). https://doi.org/10.1109/SSCI.2016.7850056
3. Beul, M., Droeschel, D., Nieuwenhuisen, M., Quenzel, J., Houben, S., Behnke, S.: Fast autonomous flight in warehouses for inventory applications. IEEE Robot. Autom. Lett. **3**, 3121–3128 (2018). https://doi.org/10.1109/LRA.2018.2849833
4. Cheeseman, I.C., Bennett, W.E.: The effect of the ground on a helicopter rotor in forward flight. Aeronautical Research Council Reports and Memoranda **3021**, 12 (1955)
5. Lee, T.E., Leishman, J.G., Ramasamy, M.: Fluid dynamics of interacting blade tip vortices with a ground plane. J. Am. Helicopter Soc. **55**, 0220051–02200516 (2010). https://doi.org/10.4050/JAHS.55.022005
6. Garofano-Soldado, A., Sanchez-Cuevas, P.J., Heredia, G., Ollero, A.: Numerical-experimental evaluation and modelling of aerodynamic ground effect for small-scale tilted propellers at low Reynolds numbers. Elsevier Masson s.r.l. (2022). https://doi.org/10.1016/j.ast.2022.107625
7. Sharf, I., Nahon, M., Harmat, A., Khan, W., Michini, M., Speal, N., Trentini, M., Tsadok, T., Wang, T.: Ground effect experiments and model validation with draganflyer x8 rotorcraft. 2014 International Conference on Unmanned Aircraft Systems, ICUAS 2014 - Conference Proceedings, 1158–1166 (2014). https://doi.org/10.1109/ICUAS.2014.6842370
8. Sanchez-Cuevas, P., Heredia, G., Ollero, A.: Characterization of the aerodynamic ground effect and its influence in multirotor control. Int. J. Aerosp. Eng. **2017** (2017). https://doi.org/10.1155/2017/1823056
9. Conyers, S.A., Rutherford, M.J., Valavanis, K.P.: An empirical evaluation of ground effect for small-scale rotorcraft. Proceedings - IEEE International Conference on Robotics and Automation 1244–1250 (2018).https://doi.org/10.1109/ICRA.2018.8461035
10. Conyers, S.A., Rutherford, M.J., Valavanis, K.P.: An empirical evaluation of ceiling effect for small-scale rotorcraft. 2018 International Conference on Unmanned Aircraft Systems, ICUAS 2018, 243–249 (2018).https://doi.org/10.1109/ICUAS.2018.8453469
11. Powers, C., Mellinger, D., Kushleyev, A., Kothmann, B., Kumar, V.: Influence of aerodynamics and proximity effects in quadrotor flight, 289–302 (2013). https://doi.org/10.1007/978-3-319-00065-7_21
12. Gao, S., Franco, C.D., Carter, D., Quinn, D., Bezzo, N.: Exploiting ground and ceiling effects on autonomous uav motion planning. 2019 International Conference on Unmanned Aircraft Systems, ICUAS 2019, 768–777 (2019). https://doi.org/10.1109/ICUAS.2019.8798091
13. Sanchez-Cuevas, P.J., Heredia, G., Ollero, A.: Multirotor uas for bridge inspection by contact using the ceiling effect. 2017 International Conference on Unmanned Aircraft Systems, ICUAS 2017, 767–774 (2017).https://doi.org/10.1109/ICUAS.2017.7991412
14. Jimenez-Cano, A.E., Sanchez-Cuevas, P.J., Grau, P., Ollero, A., Heredia, G.: Contact-based bridge inspection multirotors: Design, modeling, and control considering the ceiling effect. Ieee Robot. Autom. Lett. **4**, 3561–3568 (2019). https://doi.org/10.1109/LRA.2019.2928206
15. Nakanishi, H., Kanata, S., Goto, R., Shimomura, T.: Modeling and experimental validation for ceiling wall effect on aerodynamic characteristics of a rotor. Artif. Life Robot. (2022). https://doi.org/10.1007/s10015-022-00798-z
16. Kocer, B.B., Kumtepeli, V., Tjahjowidodo, T., Pratama, M., Tripathi, A., Lee, G.S.G., Wang, Y.: Uav control in close proximities - ceiling effect on battery lifetime. Proceedings - 2019 2nd International Conference on Intelligent Autonomous Systems, ICoIAS 2019, 193–197 (2019). https://doi.org/10.1109/ICOIAS.2019.00041
17. Conyers, S.: Empirical Evaluation of Ground, Ceiling, and Wall Effect for Small-Scale Rotorcraft. https://digitalcommons.du.edu/etd/1570
18. Sanchez-Cuevas, P.J., Heredia, G., Ollero, A.: Experimental approach to the aerodynamic effects produced in multirotors flying close to obstacles. Adv. Intell. Syst. Comput. **693**, 742–752 (2018). https://doi.org/10.1007/978-3-319-70833-1_60
19. Britcher, V., Bergbreiter, S.: Use of a mems differential pressure sensor to detect ground, ceiling, and walls on small quadrotors. IEEE Robot. Autom. Lett. **6**, 4568–4575 (2021). https://doi.org/10.1109/LRA.2021.3068661
20. David Du Mutel De Pierrepont Franzetti, I., Capello, E., Vilardi, A., Parin, R.: Experimental evaluation of wall effect for small uavs in climate-controlled environments. 2022 IEEE 9th International Workshop on Metrology for AeroSpace, MetroAeroSpace 2022 - Proceedings, 119–123 (2022). https://doi.org/10.1109/METROAEROSPACE54187.2022.9855918
21. Robinson, D.C., Chung, H., Ryan, K.: Computational investigation of micro rotorcraft near-wall hovering aerodynamics. 2014 International Conference on Unmanned Aircraft Systems, ICUAS 2014 - Conference Proceedings, 1055–1063 (2014). https://doi.org/10.1109/ICUAS.2014.6842357
22. Paz, C., Suárez, E., Gil, C., Baker, C.: Cfd analysis of the aerodynamic effects on the stability of the flight of a quadcopter uav in the proximity of walls and ground. J. Wind Eng. Ind. Aerodyn. **206** (2020). https://doi.org/10.1016/j.jweia.2020.104378
23. Carreño Ruiz, M., Bloise, N., Capello, E., D'Ambrosio, D., Guglieri, G.: Assessment of quadrotor near-wall behaviour using six-degrees of freedom cfd simulations. (2023). https://doi.org/10.2514/6.2023-2272
24. Garofano-Soldado, A., Heredia, G., Ollero, A.: Aerodynamic interference in confined environments with tilted propellers: Wall effect and corner effect. Institute of Electrical and Electronics Engineers Inc., (2021). https://doi.org/10.1109/AIRPHARO52252.2021.9571031
25. David Du Mutel De Pierrepont Franzetti, I., Parin, R., Capello, E.: Wall effect evaluation of small quadcopters in pressure-controlled environments. 2023 International Conference on Unmanned Aircraft Systems, ICUAS 2023, 1142–1147 (2023). https://doi.org/10.1109/ICUAS57906.2023.10156365
26. Scanavino, M., Vilardi, A., Guglieri, G.: An experimental analysis on propeller performance in a climate-controlled facility. J. Intell. Robot. Syst. Theory Appl. **100**, 505–517 (2020). https://doi.org/10.1007/s10846-019-01132-9

27. Scanavino, M., Avi, A., Vilardi, A., Guglieri, G.: Unmanned aircraft systems performance in a climate-controlled laboratory. J. Intell. Robot. Syst. Theory Appl. **102** (2021). https://doi.org/10.1007/s10846-021-01392-4
28. Bojeri, A., Mai, E., Ristorto, G., Parin, R., Vilardi, A., Guglieri, G.: Characterisation of unmanned aerial vehicle performance under extreme environmental conditions in a controlled atmospheric facility. 2022 International Conference on Unmanned Aircraft Systems, ICUAS 2022, 1030–1039 (2022). https://doi.org/10.1109/ICUAS54217.2022.9836145
29. Parin, R., Bojeri, A., Benedetto, F., Ristorto, G., Guglieri, G.: Unmanned aerial vehicles experimental characterization in controlled extreme environmental conditions. 2023 International Conference on Unmanned Aircraft Systems, ICUAS 2023, 658–662 (2023). https://doi.org/10.1109/ICUAS57906.2023.10155932
30. Scanavino, M.: Design and testing methodologies for uavs under extreme environmental conditions. PhD thesis, Politecnico di Torino (2021)
31. Axis Load Cell Systems, J.M.: Specification sheet 30e15 f/t sensor. (2019)
32. ATI Industrial Automation: F/T Sensor Mini40. https://www.ati-ia.com/products/ft/ft_models.aspx?id=mini40 Accessed 2013-11-15
33. WLA16P-24162100A00 - W16 | SICK. https://www.sick.com/us/en/catalog/products/detection-sensors/photoelectric-sensors/w16/wla16p-24162100a00/p/p512654. Accessed 16 Nov 2013
34. Russell, C., Willink, G., Theodore, C., Jung, J., Glasner, B.: Wind tunnel and hover performance test results for multicopter UAS vehicles (2018). http://www.sti.nasa.gov
35. BIPM, IEC, IFCC, ILAC, ISO, IUPAC, IUPAP, OIML: Evaluation of measurement data — Guide to the expression of uncertainty in measurement. Joint Committee for Guides in Metrology, JCGM 100:2008. https://www.bipm.org/documents/20126/2071204/JCGM_100_2008_E.pdf/cb0ef43f-baa5-11cf-3f85-4dcd86f77bd6
36. Supplementary Information Repository. https://doi.org/10.5281/ZENODO.11384638. https://zenodo.org/records/11384638

Iris David Du Mutel de Pierrepont Franzetti is a PhD student in the fields of UAV and robotics. She studied her Bachelor's degree in Aerospace Engineering at the University of Seville, and a Master's degree in Aerospace Science and Technology in the Polytechnic University of Catalonia. She participated in the Erasmus+ program, to do her Master thesis in the Polytechnic University of Turin on Guidance and Control Algorithms for UAV Indoor Applications. After, she dedicated a year as fellow research assistant in robotics modelling and simulation as well as UAV control systems within a PRIN program. On November 2021, she started a PhD program about UAV control and disturbance modelling with a strong experimental component in collaboration with TerraXcube facilities at EURAC Research, Bolzano.

Riccardo Parin received hir Masters degree in Energy Engineering (2015) and PhD in Industrial Engineering (2018) at the University of Padova, Italy. His PhD work focused on experiments on two-phase heat transfer processes on nano-structured metal surfaces with different wettablities under the supervision of Prof. Davide Del Col. In 2019-2020 he worked as a post-doctoral fellow at the University of Sydney in the School of Chemistry in the group of Prof. Chiara Neto and in collaboration with Prof. Martijn de Sterke (Physics Department), working on the ACWA (Advanced Capture of Water from the Atmosphere) project. The project focused on developing a low-cost method to capture enough water from the atmosphere to alleviate the effect of drought by providing water for consumption by humans and animals, and for irrigating plants. Author of different scientific journal articles and winner of the CDIP fund of the University of Sydney.

Elisa Capello is Full Professor of Flight Mechanics at Politecnico di Torino, Department of Mechanical and Aerospace Engineering. She is research associate at the Istituto di Elettronica e di Ingegneria dell'Informazione e delle Telecomunicazioni (IEIIT) of the Italian National Research Council (CNR), in the Systems Modeling and Control group (http://www.sct.ieiit.cnr.it) since 2012. She is a member of The Institute of Electrical and Electronics Engineers, Member (IEEE), Control Systems Society since 2014. She is a member of the IEEE Technical Committee in Aerospace Control since 2016.

Author of more than 100 papers published in international journals and conferences of the following sectors: aerospace engineering, control, automation and robotics. She is involved in research activities in the following fields: design of guidance, control and navigation systems for aircraft and spacecraft, control of wind turbine and wind farm, flight mechanics of fixed and rotary wing aircraft, testing of unmanned aerial systems, planning and mission control for autonomous systems. As part of her research activities, she collaborates with academic institutions, research centers, networks and companies, both in Italy and abroad. Elisa Capello was an International FAI Judge for Helicopter Championship from 2009 to 2015.

Matthew J. Rutherford received the B.S. degree in civil engineering from Princeton University, in 1996 and the M.S. and Ph.D. degrees in computer science from the University of Colorado, Boulder, in 2001 and 2006, respectively. He is currently an Associate Professor with the Department of Computer Science with a joint appointment with the Department of Electrical and Computer Engineering, University of Denver, Denver, CO, USA, where he is also the Deputy Director of the DU Unmanned Systems Research Institute (DU2SRI). His research interests include the development of advanced controls and communication mechanisms for autonomous aerial and ground robots; applications of real-time computer vision to robotics problems using GPU-based parallel processing; testing and dynamic evaluation of embedded, real-time systems; development of complex mechatronic systems (mechanical, electrical, and software); the development of software techniques to reduce the amount of energy being consumed by hardware; development of a high-precision propulsion system for underwater robots.

Dr. Kimon P. Valavanis joined the University of Denver in September 2008 as Professor and Chair of the Electrical and Computer Engineering Department. He is currently John Evans Professor, Director of Research and Innovation at the D. F. Ritchie School of Engineering and Computer Science, and Founding Director of the Unmanned Systems Research Institute. He is also Guest Professor in the Faculty of Electrical Engineering and Computing at the University of Zagreb, Croatia. He also was chosen by the Academic Senate and the Board of Governors of the Politecnico di Torino to collaborate in research and offer a series of seminars and short course in Robotics and Unmanned Systems under the Scuola di Dottorato program requirements as part of the European Research Council (ERC), European Commission, Horizon 2020 Scientific Programme, Part 1 - Excellent Science. Valavanis has offered similar courses at: Università Politecnica delle Marche, Ancona, Italy; South China University of Technology; Technion University, Israel; Universidade Federal do Espírito Santo (UFES), Vittoria, Brazil; Latin American and Brazilian Robotics Competition, João Pessoa, Brazil; Poznan Institute of Technology, Poland; Technical University of Crete and National Technical University of Athens, Greece. During his 30+ years of Academic career, Valavanis has graduated 38 PhD students and more than 100 M.Sc. students. He has attracted and has helped attracting close to $50M in research funds from Federal and State agencies, industry and the private sector. While in Europe, he was funded by the Greek Secretariat of Research and Technology, the European Union, industry, and from the Croatian Ministry of Science and Technology (joint projects).

Valavanis' research interests focus on the areas of Unmanned Systems, Distributed Intelligence Systems, Robotics and Automation. He has published more than 400 book chapters, technical journal, referred conference papers, invited papers and technical reports. He has authored, co-authored and edited 19 books, two of which have been translated in Chinese. He has organized international conferences, worldwide. He was Editor-in-chief (EIC) of the IEEE Robotics and Automation Magazine for ten years; EIC of the IEEE Systems Man and Cybernetics Newsletter for three years; EIC of the Journal of Intelligent and Robotic Systems since 2006. He serves as co-chair/chair of the Aerial Robotics and Unmanned Aerial Vehicles Technical Committee since 2008. He serves since 1998 as Vice President of the Mediterranean Control Association.

Dr. Valavanis has received invitations by the Hellenic Quality Assurance Agency (H.Q.A.A.) for Higher Education of the Hellenic Republic to evaluate Greek Universities (ABET Evaluation), and by the European Union to be an evaluator of IP and STREP projects as part of the 7th European Union (EU) Framework Programme for Research and Technology Development (FP7) - Information and Communication Technologies (ICT-2009.2.1 Cognitive Systems and Robotics), and he also served as a member of the Hearing Committee panel in Luxembourg. He is an appointed Scientific Project Reviewer in projects financed by the Ministry of Science, Education and Sports of the Republic of Croatia and in research projects evaluated by the Italian Evaluation of Research Quality exercise (VQR 2004-2010).

Dr. Valavanis was a Distinguished Speaker in the IEEE Robotics and Automation Society; Senior Member of IEEE; Fellow of the American Association for the Advancement of Science; Fellow of the U.K. Institute of Measurement and Control; Fulbright Scholar (Senior Lecturing & Research Award), and, Technical Expert of the NATO Science and Technology Organization (STO). In May of 2019, during the 25-year anniversary meeting for the Robotics and Automation Magazine, he was awarded by IEEE and the Robotics and Automation Society for his 10 years of service as Editor-in-Chief.

Authors and Affiliations

Iris David Du Mutel de Pierrepont Franzetti[1,2] · Riccardo Parin[2] · Elisa Capello[3] · Matthew J. Rutherford[4] · Kimon P. Valavanis[5]

✉ Iris David Du Mutel de Pierrepont Franzetti
iris.daviddu@polito.it

Riccardo Parin
riccardo.parin@eurac.edu

Elisa Capello
elisa.capello@polito.it

Matthew J. Rutherford
matthew.rutherford@du.edu

Kimon P. Valavanis
kimon.valavanis@du.edu

1 Department of Mechanical and Aerospace Engineering, Politecnico di Torino, Corso Duca degli Abruzzi 24, Torino 10129, Italy

2 terraXcube, Eurac Research, Via Ipazia 2, Bolzano 39100, Italy

3 Department of Mechanical and Aerospace Engineering, Politecnico di Torino, CNR/IEIIT, Corso Duca degli Abruzzi 24, Torino 10129, Italy

4 Department of Computer Science, University of Denver, 2155 E. Wesley Ave., Denver, CO 80208, USA

5 Department of Electrical & Computer Engineering, University of Denver, 2155 E. Wesley Ave., Denver 80208, CO, USA